Realization of Mg^{2+} intercalation in a thermodynamically stable layer-structured oxide

Zunhao Zhang, [ab] Haotian Guan, [ab] Jili Yue, *[ab] Yangfan Lu, [ab] Qian Li, [ab] Guangsheng Huang, [ab] Jingfeng Wang, [ab] Baihua Qu *[ab] and Fusheng Pan

[a]College of Materials Science and Engineering, National Engineering Research Center for Magnesium Alloys, National Innovation Center for Industry-Education Integration of Energy Storage Technology, Chongqing University, Chongqing, 400044, China.

E-mail: jili.yue@cqu.edu.cn, bhqu@cqu.edu.cn

[b]Chongqing Institute of New Energy Storage Materials and Equipment, Chongqing 401135, China

Experimental section

Synthesis of Materials

$Na_{0.67}MnO_2$ (NMO) and $K_{0.5}MnO_2$ (KMO) were synthesized by conventional solid-state reaction method. K_2CO_3 (99.99%, Shanghai Aladdin Biochemical Technology Co., Ltd.). Na_2CO_3 (99%, Shanghai Aladdin Biochemical Technology Co., Ltd). Mn_2O_3 (98%, Shanghai Aladdin Biochemical Technology Co., Ltd) were used as precursors. The raw materials were weighed according to the target molar ratio, with a 5 % excess of K_2CO_3 (or Na_2CO_3) to compensate for the loss of K (Na) during high-temperature calcination, and then mixed and ground in an agate mortar for 30 min, placed in a ball mill for 4 hours at 300 rpm. After the well-mixed powder was pressed into a pellet with a height of 5 mm and a diameter of 10 mm, the above pellet was placed in a crucible and calcined in a muffle furnace at 900℃ for 12 h. The material was then quickly

transferred to an argon-filled glovebox for sealing when the furnace was cooled down to 100 ℃.

Characterization

The XRD data of the KMO and NMO materials were measured at room temperature using (Bruker D8 Advance) and Cu-α radiation, testing diffraction angle angles (2θ) of 10°-70°. The micro-morphology of the samples was observed and analyzed using a scanning electron microscopy (ZEISS Gemini SEM 300, Germany). Changes in ion valence states in the samples before and after Mg^{2+} embedding were analyzed by X-ray photoelectron spectroscopy (Thermo Scientific K-Alpha, USA). The transmission electron microscopy (TEM) images and energy dispersive spectrometer (EDS) mapping of samples were carried out by JEOL JEM-F200.

Preparation of APC and MACT electrolytes

0.4 $_M$ APC: All the synthesis was done in an argon filled glove box. Firstly, 0.267g of $AlCl_3$ (Aldrich, 99.99%) powder was added in 3mL tetrahydrofuran (THF, Aldrich, 99.9%), the solution was then stirred for 8h. Finally, 2 mL of the PhMgCl THF solution (Macklin, 2 mol L^{-1}) was added to the above solution and stirred overnight to obtain a clarified electrolyte.

0.25 $_M$ MACT: All the synthesis was done in an argon filled glove box. The MACT ($MgCl_2$/$AlCl_3$/$Mg(TFSI)_2$,2/1/1) electrolyte is prepared according to a previous report.[1] Firstly, 0.095g of $MgCl_2$ (Macklin, 99.9%) powder was added into 2mL 1,2-dimethoxyethane (DME) (Macklin, 99.5%) while stirring, then 0.0663g of $AlCl_3$ (Alfa, 99.99%) and 0.293g of magnesium bis(trifluoromethanesulfonyl)imide ($Mg(TFSI)_2$)

(Macklin, 97%) powders were added into above solution in order. After stirring for 12 h in argon filled glove box, 0.25 $_M$ MACT electrolyte was obtained.

Electrochemical Measurements

The electrochemical properties of both cathodes were obtained from Swagelok cell measurements. NMO and KMO electrode sheets were prepared in an argon-filled glove box to avoid the contamination of moisture. NMO (KMO) electrode material (70 wt%), Super P carbon black (20 wt%) and dry PTFE (polytetrafluoroethylene 10 wt%) were ground in a mortar and pestle, and after a few minutes, a uniform sheet was obtained, and the obtained dry electrode sheet was cut with scissors into several small pieces with a mass of 5-8 mg for spare use. The polished magnesium foils with a diameter of 12 mm were used for anode, and the electrolyte was 0.4 $_M$ APC and 0.25 $_M$ MACT, and all the battery assembly processes were carried out in an argon-filled glove box, where the water and oxygen content was less than 0.1 ppm. Galvanostatic charge/discharge was carried out using the NEWARE software in the voltage range of 1.0-3.1 V. The battery was then charged and discharged using the NEWARE software in a constant-current mode. For the cyclic voltammetry (CV) and electrochemical impedance spectroscopy (EIS) test, the cells were constructed using the as-prepared material as the working electrode and Mg foil as the counter electrode, respectively. CV tests were performed on an electrochemical workstation CHI 660B in the potential range of 1.0–3.1 V vs. Mg^{2+}/Mg at the scan rates of 0.1 mV s^{-1}. EIS, with a voltage amplitude of 5 mV and a frequency range of 10^5 Hz to 0.01 Hz, was used to evaluate the electrode processes.

Calculation method

Density functional theory (DFT) calculations were implemented in the Vienna ab-initio simulation package (VASP).[2] In these calculations, we utilized the Perdew−Burke−Ernzerhof (PBE)[3] functional within the framework of the generalized gradient approximation (GGA)[4], and the description of core electrons was facilitated by the projector augmented wave (PAW) method. The $Na_{0.67}MnO_2$ and $K_{0.5}MnO_2$-supercells were constructed based on the optimized bulk lattice parameters, and the supercell were modeled by a 3×3×1 unit cell. A 20-Å-thick vacuum region was set to prevent interaction between slabs. A cutoff energy of 520 eV and a Monkhorst–Pack K-mesh setting of 5×5×1 were employed in the structural optimization. The convergence criteria for energy and force were respectively 10^{-6} eV and 0.01 eV/Å. To simulate the migration process of Mg in different host, some atoms were removed from each Na or K layer in the supercells. The energy barrier for Mg^{2+} migration was evaluated using the climbing nudged elastic band (CI-NEB) methods.

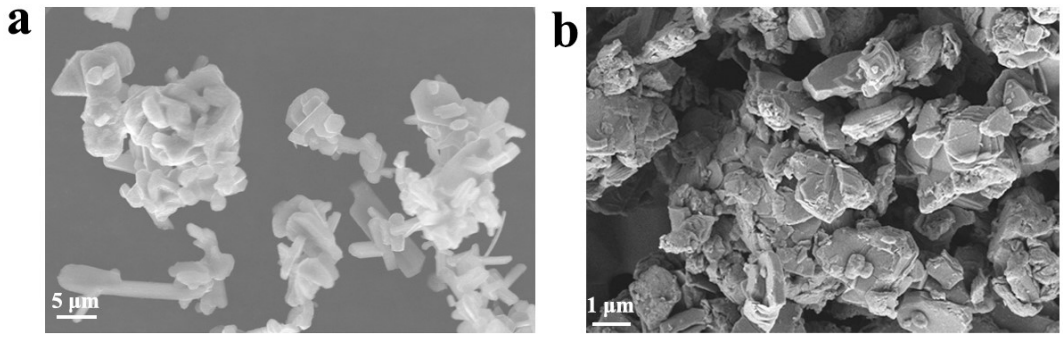

Fig. S1 SEM images of the as synthesized (a) NMO and (b) KMO.

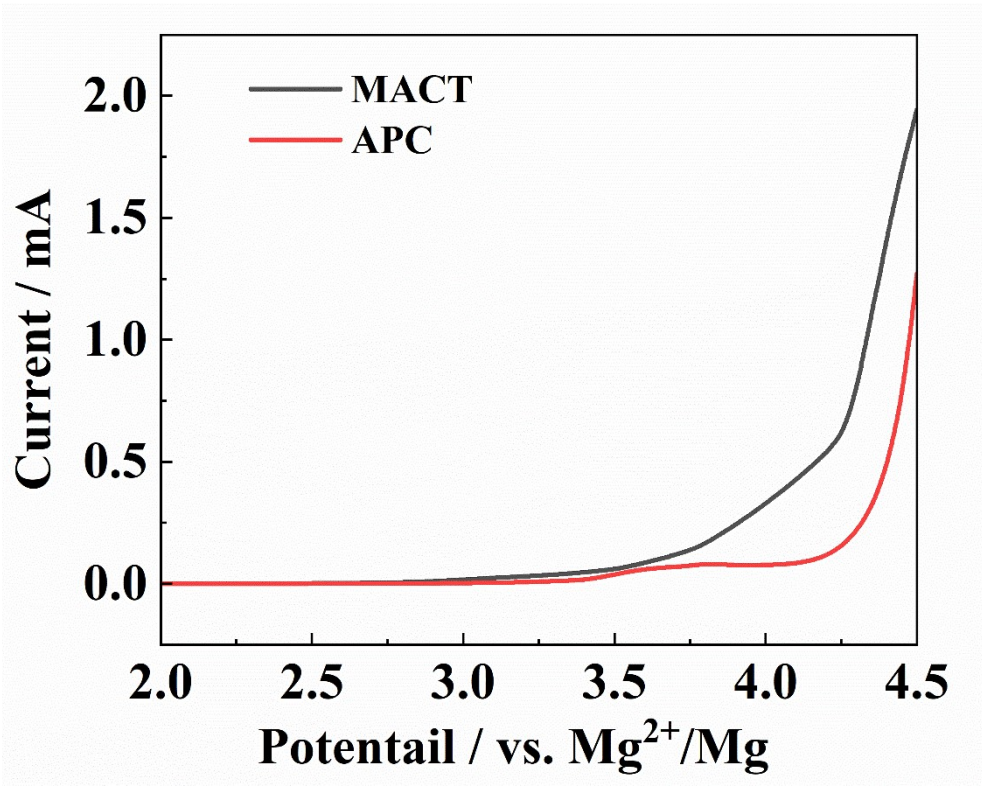

Fig. S2 Linear sweep voltammetry curves of the APC and MACT electrolytes using Mo electrode.

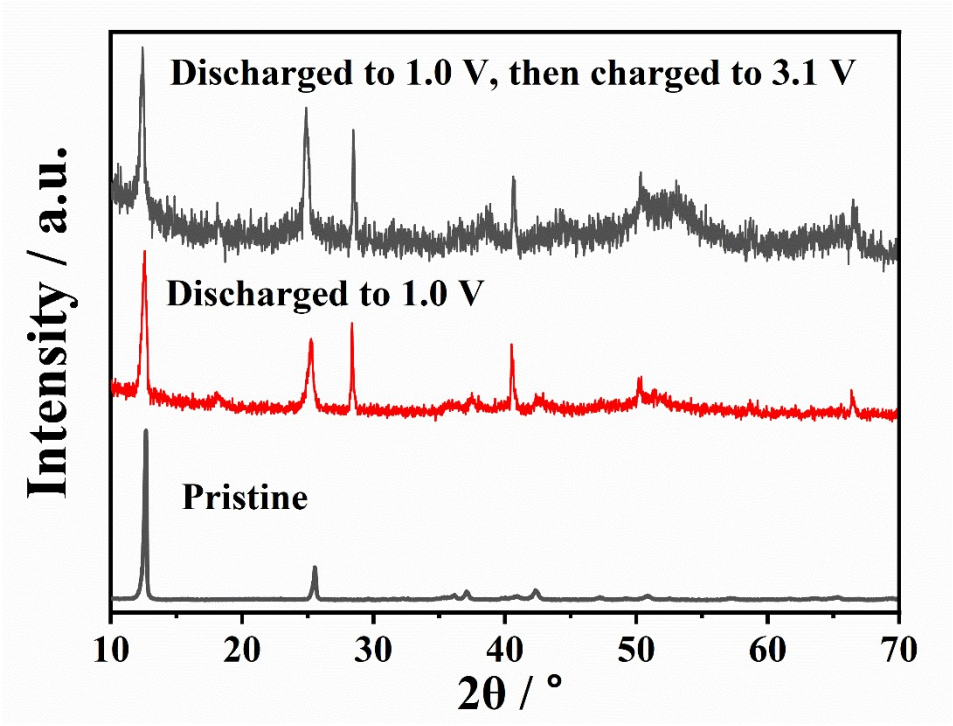

Fig. S3 The XRD patterns of the fully discharged and re-charged KMO electrodes.

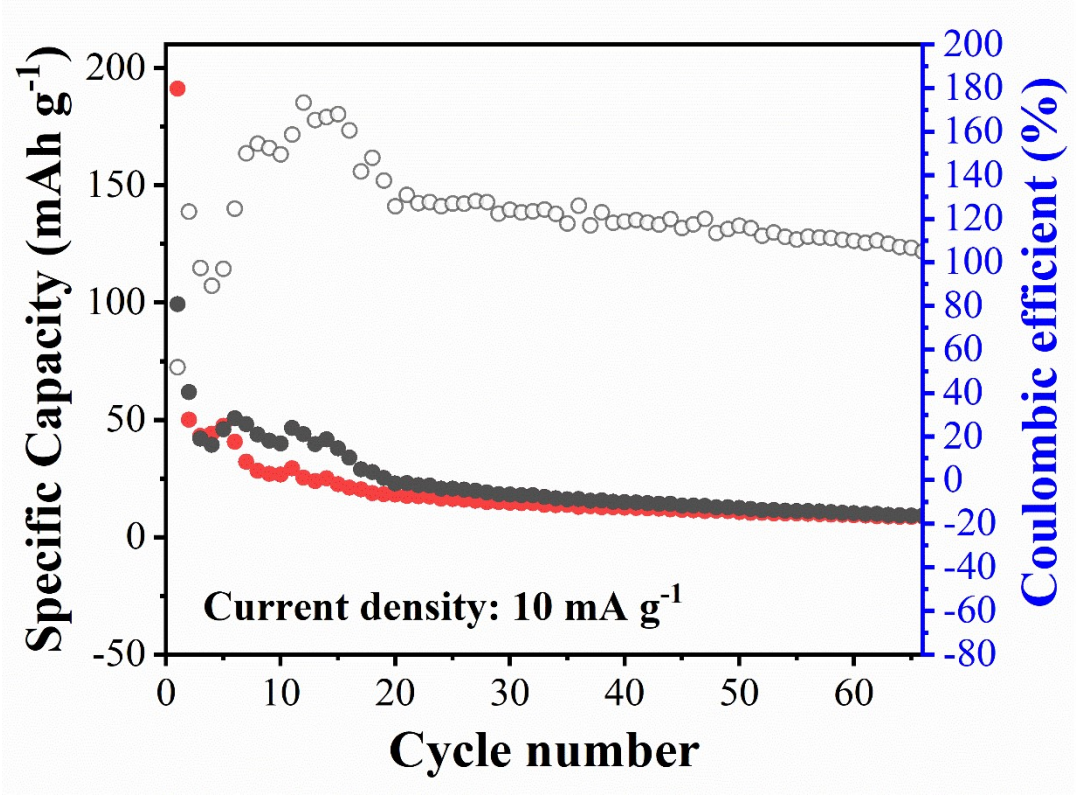

Fig. S4 Cycling performance of KMO in MACT at 10 mA g^{-1}.

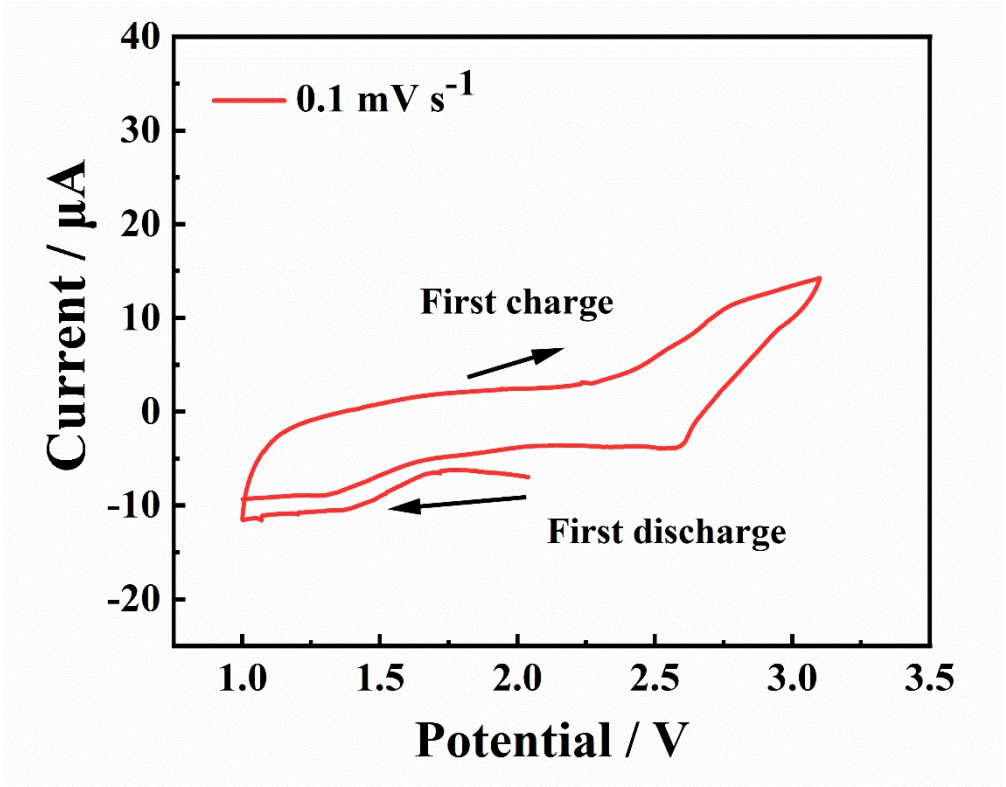

Fig. S5 Cyclic voltammetry (CV) curve of KMO in MACT in the potential range of 1.0–3.1 V vs. Mg^{2+}/Mg at the scan rates of 0.1 mV s^{-1}.

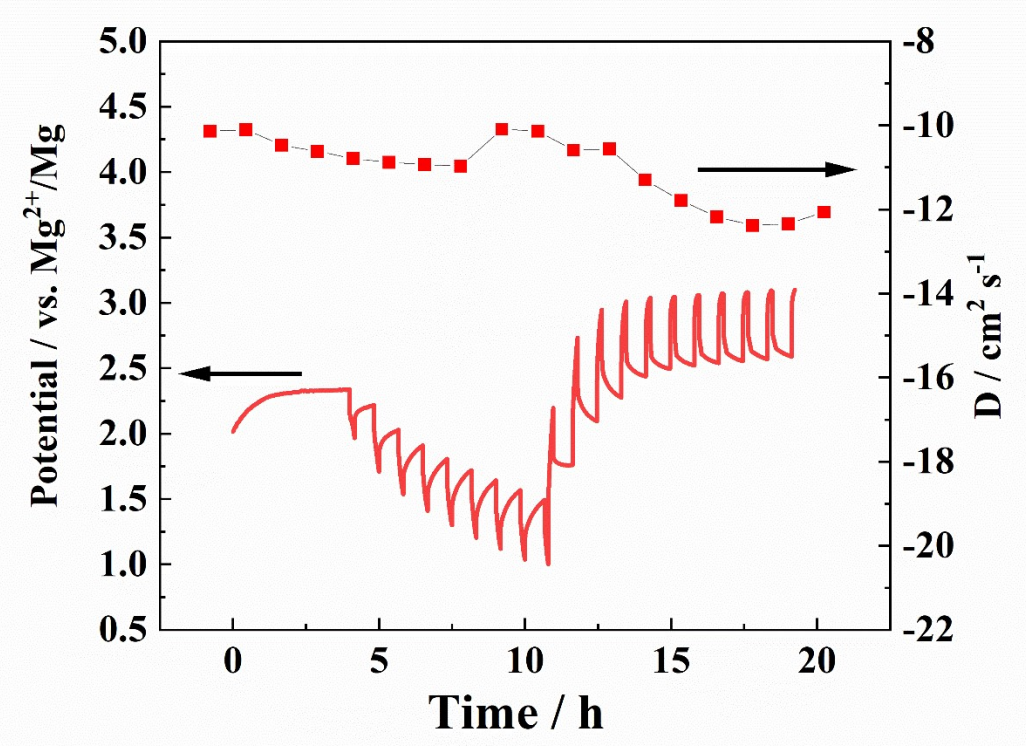

Fig. S6 Galvanostatic intermittent titration technique (GITT) of KMO in MACT and diffusion coefficient of Mg^{2+} ($D_{Mg^{2+}}$) from GITT.

The calculation of diffusion coefficient of Mg^{2+} ($D_{Mg^{2+}}$) from GITT was according to the following equation[5]:

$$D_{Mg^{2+}} = \frac{4}{\pi\tau}\left(\frac{n_m V_m}{S}\right)^2 \left(\frac{\Delta E_s}{\Delta E_t}\right)^2$$

where τ is the constant current pulse time, V_m and n_m are the molar volume and molar mass of the active materials, respectively, and S represents the electrode surface area. ΔE_s is the change value of balanced voltage and ΔE_t is the voltage change during the current pulse, respectively.

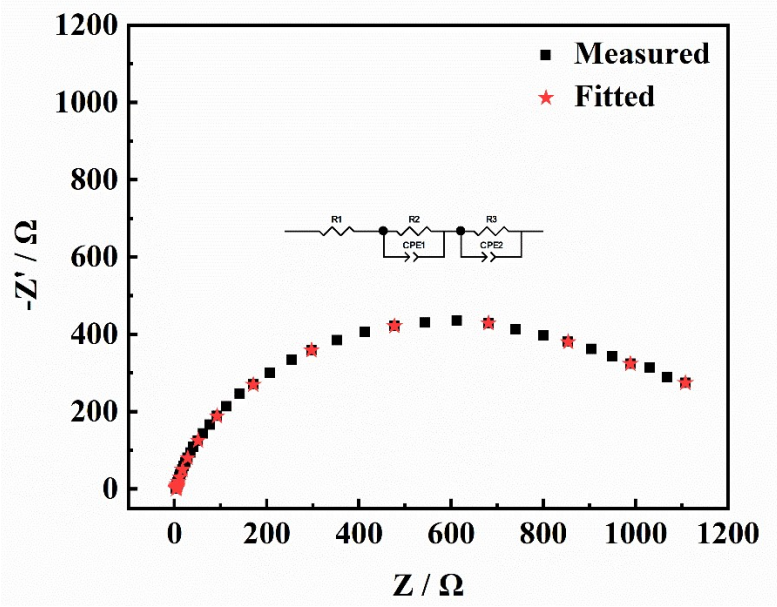

Fig. S7 The Nyquist plots of electrochemical impedance spectroscopy (EIS) at OCP for KMO.

The equivalent circuit element R_{Ω} (the intercept with the x-axis at high frequencies) corresponds to the Ohmic resistance of the cell, which is dominated by resistance of electrolyte; the R_{ct} (the intercept with the x-axis at medium frequencies) is likely associated with the charge transfer (ct) processes (or the kinetics of the redox reactions); and R_{mt} (the intercept with the x-axis at the low frequency zone) corresponds likely to the resistance to mass transfer (mt) processes (e.g., diffusion of Mg^{2+} ions in response to electrode reactions). The CPE1 and CPE2 are the constant phase elements associated with the charge and mass transfer processes, respectively, which have been used instead of capacitors to take into account the influence of particle size distribution, electrode tortuosity, and surface roughness[5-7].

$D_{Mg^{2+}}$ can be calculated by the following equation:

$$D_{Mg^{2+}} = \frac{R^2T^2{R_{mt}}^2}{n^4F^4A^2C^2}$$

where, R is ideal gas constant, T is absolute temperature (K), n is electron transfer number, F is Faraday constant, A is electrode area, C is the concentration of Mg^{2+} in the lattice.

Table S1 Comparison of electrochemical performance of other materials with the respective samples.

Materials	Electrolyte	Specific capacity	Current density	Anode	Reference
PEO-V_2O_5	$Mg(ClO_4)_2$/AN	130 mAh g^{-1}	10	AC	(8)
α-MoO_3	$Mg(ClO_4)_2$/AN+3mol% H_2O	210 mAh g^{-1}	not shown	AC	(9)
V_2O_5	$Mg(ClO_4)_2$+1.79 mol L^{-1} H_2O/PC	158.6 mAh g^{-1}	0.3 mA cm^{-2}	Mg	(10)
$Mg_{0.3}V_2O_5{\cdot}1.1H_2O$	0.3 M $Mg(TFSI)_2$/AN	164 mAh g^{-1}	100mAg^{-1}	AC cloth	(11)
Birnessite-MnO_2	0.5 M $Mg(ClO_4)_2$	110.8 mAh g^{-1}	232.69 mA g^{-1}	Ag/AgCl electrode	(12)
MgV_2O_4	$Mg(TFSI)_2$/PY_{14}TFSI	45 mAh g^{-1}	not shown	AC and Mg foil	(13)
$MgMn_2O_4$	$Mg(TFSI)_2$/DME	158 mAh g^{-1}	10 mA g^{-1}	Mg foil	(14)
$MgMn_2O_4$	0.3M $Mg[B(HFIP)_4]_2$/ triglyme	270mAh g^{-1}	10 mA g^{-1}	AZ-31	(15)
$K_{0.5}MnO_2$	$MgCl_2/AlCl_3/Mg(TFSI)_2$ in DME	99 mAh g-1	10 mA g^{-1}	Mg	This work

Note for Table S1:

Majority of reported results are based on metastable nanoscale materials, H_2O or other molecules inserted materials, using three electrode system, or active carbon anode, this work utilizes thermodynamically stable $K_{0.5}MnO_2$ as cathode, through optimized electrolytes, realizing Mg^{2+} intercalation into $K_{0.5}MnO_2$ framework in a real magnesium battery directly using Mg foil as anode.

Table S2 Crystallographic parameters of KMO deduced from Reference 16 and 17.

Atom	Occupancy	x	y	z
K	0.5	0.5	0.2	0.5
Mn	1.0	0	0	-0.01(2)
O	1.0	2/3	1/3	0.11(6)

Space group: R3m (No.160) a=b=2.882 Å c=19.350 Å

Table S3 Crystallographic parameters of NMO deduced from Reference 18.

Atom	Occupancy	x	y	z
Na	0.26	0.0	0.0	0.25
Na	0.40	2/3	1/3	0.75
Mn	1.0	0.0	0.0	0.0
O	1.0	2/3	1/3	0.076

Space group: P63/mmc (No.160) a=b=2.8708 Å c=11.1735 Å

References

(1) L. Yang, C. Yang, Y. Chen, Z. Pu, Z. Zhang, Y. Jie, X. Zheng, Y. Xiao, S. Jiao, Q. Li, D. Xu, . *ACS Appl. Mater. Interfaces,* 2021, **13**, 30712-30721.

(2) G. Kresse and J. Furthmuller, *Phys. Rev. B,* 1996, **54**, 11169-11186.

(3) P. E. Blöchl, *Phys. Rev. B*, 1994, **50**, 17953-17979.

(4) J. P. Perdew, M. Ernzerhof and K. Burke, *J. Chem. Phys.,* 1996, **105**, 9982-9985.

(5) T. Yuan, S. Li, Y. Sun, J. -H. Wang, A. J. Chen, Q. Zheng, Y. Zhang, L. Chen, G. Nam, H Che, J. Yang, S. Zheng, Z. Ma and M. Liu, *ACS Nano* 2022, **16**, 18058‑18070.

(6) R. Shanmugam and W. Lai *J. Electrochem. Soc.,* 2015, **162**, A8-A14

(7) J. Yue, Y. Zhou, X. Yu, S. Bak, X. Yang and Z. Fu, *J. Mater. Chem. A*, 2015, **3**, 23261–23267.

(8) A. Mukherjee, S. Taragin, H. Aviv, I. Perelshtein and M. Noked, *Adv. Funct. Mater.,* 2020, **30**, 2003518.

(9) M.E. Spahr, P. Novak, O. Haas and R. Nesper, *J. Power Sources*, 1995, **54,** 346-351.

(10) L. Yu and X. Zhang, *J. Colloid Interface Sci.,* 2004, **278,** 160–165.

(11) Y. A. Xu, X. W. Deng, Q. D. Li, G. B. Zhang, F. Y. Xiong, S. S. Tan, Q. L. Wei, J. Lu, J. T. Li, Q. Y. An and L. Q. Mai, *Chem* 2019, **5**, 1194–1209.

(12) M. Q Wang and S. Yagi, *J. Alloy. Comp.* 2020, **820**, 153135.

(13) L. Hu, J. Jokisaari, B. Kwon, L. Yin, S. Kim, H. Park, S. Lapidus, R. Klie, B. Key, P. Zapol, B. Ingram, J. Vaughey and J. Cabana, *ACS Energy Lett*. 2020, **5**, 2721−2727.

(14) R. Ruiz, C. Vicente, S. Rubioa, R. Stoyanova, W. Zuo, Y. Yang and G. Ortiz, *Energy Storage Mater.*, 2022, **48**, 12–19.

(15) H. Kobayashi, Y. Fukumi, H. Watanabe, R. Iimura, N. Nishimura, T. Mandai, Y. Tominaga, M. Nakayama, T. Ichitsubo, I. Honma and H. Imai, *ACS Nano* 2023, **17**, 3135 −3142.

(16) R. Luo, X. Li, J. Ding, J. Bao, C. Ma, C. Du, X. Cai, X. Wu, Y. Zhou, *Energy Storage Mater.* 2022, **47**, 408-414.

(17) J. Weng, J. Duan, C. Sun, P. Liu, A. Li, P. Zhou, J. Zhou, *Chem. Eng. J.* 2020, **392**, 123649.

(18) W. Zuo, J. Qiu, X. Liu, B. Zheng, Y. Zhao, J. Lia, H. He, K. Zhou, Z. Xiao, Q. Li, G. F. Ortiza, Y. Yang, *Energy Storage Mater.* 2020, **26**, 503-512.